



1 **Freeze-thaw processes correspond to the protection-loss of soil**
2 **organic carbon through regulating pore structure of aggregates**
3 **in alpine ecosystems**

4 Ruizhe Wang^{1,2}, Xia Hu^{1,2*}

5

6 1 State Key Laboratory of Earth Surface Processes and Resource Ecology, Faculty of Geographical Science, Beijing
7 Normal University, Beijing 100875, China.

8 2 School of Natural Resources, Faculty of Geographical Science, Beijing Normal University, Beijing 100875, China.

9 *Correspondence* to: Xia Hu (huxia@bnu.edu.cn, +86-010-58800238)

10



11 **Abstract.** Seasonal freeze–thaw (FT) processes alter soil formation and causes changes in soil structure in alpine
12 ecosystems. Soil aggregates are basic soil structural units and play a crucial role in soil organic carbon (SOC)
13 protection and microbial habitation. However, the impact of seasonal FT processes on pore structure and its impact
14 on SOC fractions have been overlooked. This study characterized the pore structure and SOC fractions of aggregates
15 during the unstable freezing period (UFP), stable frozen period (SFP), unstable thawing period (UTP) and stable
16 thawed period (STP) in typical alpine ecosystems via the dry sieving procedure, X-ray computed tomography (CT)
17 scanning and elemental analysis. The results showed that pore characteristics of 0.25-2 mm aggregates were more
18 vulnerable to seasonal FT processes than that of > 2 mm aggregates. The freezing process promoted the formation of >
19 80 μm pores of aggregates. The total organic carbon (TOC), particulate organic carbon (POC) and mineral-associated
20 organic carbon (MAOC) contents of macroaggregates were high in the stable frozen period and low in unstable
21 thawing period, demonstrating that freezing process enhanced SOC accumulation while early stage of thawing led to
22 SOC loss. The vertical distribution of SOC of aggregates was more uniform in stable frozen period than in other
23 periods. Pore equivalent diameter was the most important structural characteristic influencing SOC contents of
24 aggregates. In the freezing period, the importance of pore structure in regulating SOC protection was more obvious
25 and pore structure inhibited SOC loss by promoted the formation of >80 μm pores. In the thawing period, pores of 15-
26 30 μm inhibited SOC protection. Our results are valuable for evaluating potential changes in alpine soil carbon sinks
27 under global warming.

28

29 **Key words:** Seasonal freeze–thaw process, soil aggregate, soil organic carbon, soil pore

30



31 **1. Introduction**

32 Freeze–thaw (FT) cycles are main process of soil formation in alpine regions and more than half of the Northern
33 Hemisphere’s soil is affected by FT cycles (Wang et al., 2007). Ongoing global warming has reduced snow cover in
34 winter and decreased the insulations of soils against freezing, which has increased the frequency of FT cycles
35 (Kreyling et al., 2008). The expansion of water volume with freezing and the shrinkage after thawing destroys soil
36 aggregates and soil organic carbon (SOC) protection (Oztas and Fayetorbay, 2003; Tan et al., 2014). FT processes not
37 only affect the stability of soil aggregates but also change their inner pore characteristics, especially those of the water-
38 filled pores (Wang et al., 2012; Li and Fan, 2014; Starkloff et al., 2017). A decrease in pore connectivity and an
39 increase in elongated porosity were observed after continuous FT events (Ma et al., 2020; Rooney et al., 2022). FT
40 cycles could lead to opposite changes in soil porosity of exterior aggregates and interior aggregates (Zhao and Hu,
41 2023a). FT processes have profound effects on the carbon cycles, accelerating the loss and decomposition of SOC in
42 the soil carbon pool of terrestrial ecosystems (Yi et al. 2015). FT processes can change SOC distribution by stimulating
43 substrate release (Song et al., 2017), destroying soil aggregates and affecting microbial activities (Campbell et al.,
44 2014; Xiao et al., 2019). The impact of FT processes on SOC fraction contents varies due to the differences in their
45 formation pathways and physio-chemical stabilities. FT processes could significantly increase soil soluble carbon
46 content and extractable SOC content but decrease microbial biomass carbon (MBC) (Patel et al., 2021). However,
47 these related studies were mostly based on simulated indoor freeze–thaw experiments. The differences between
48 simulated FTC conditions and field FT conditions are in that (1) the indoor FTC cannot simulate the dynamics of
49 vegetation growth, which had significant impacts on SOC origin and soil structure and (2) the indoor FTC cannot
50 reflect the changes in environmental factors which impacts the FT conditions. Quantifying pore structure and SOC
51 fractions of soil aggregates during the seasonal FT process is valuable for understanding how freezing and thawing
52 affect soil structure and functions.

53 Soil structure refers to the spatial arrangement of solids and voids and controls many important biophysical
54 processes in soils (Rabot et al., 2018). Soil aggregates are basic units of soil and are important indicators of soil
55 structure and soil quality (Six et al., 2000; 2004). According to their diameters, soil aggregates can be divided into
56 microaggregates (< 0.25 mm) and macroaggregates (> 0.25 mm). Macroaggregates play a key role in stabilizing SOC,
57 maintaining levels of water and nutrients and microbial habitation (Ananyeva et al., 2013; Chen et al., 2019; Wang et
58 al., 2022). SOC is preserved by physical protection in the forms of light organic carbon (fLOC), particulate organic
59 carbon (POC) and mineral-associated organic carbon (MAOC). POC is a crucial contributor to soil aggregation and
60 parallels plant-derived carbon into aggregates, and MAOC plays a crucial role in long-term SOC storage (Wang et al.,



61 2020; Witzgall et al., 2021). This classification benefits a more extensive understanding of soil carbon maintenance
62 and response to climate change and land use (Kallenbach et al., 2016; Lavalley et al., 2020; Liao et al., 2023). The
63 pore networks of soil aggregates are heterogeneous. They can directly influence the accessibility of organic matter to
64 microbes and indirectly influence microbial activities, thus determining the magnitude to which the SOC is protected
65 (Ruamps et al., 2013; Kravchenko and Guber, 2018). Interactions between pore structure and SOC soil aggregates
66 have gained much attention. Zhang et al. (2023) proposed that pore structure alone explained 6.41% and 12.64% of
67 the variation in the SOC of aggregates in the topsoil and subsoil, respectively. Pores of 30-75 μm and $> 13 \mu\text{m}$ in
68 size were found to enhance the mineralization of carbon (Lugato et al., 2009; Kravchenko et al., 2015). Pores of > 90
69 μm (Quigley and Kravchenko., 2022) and $< 15 \mu\text{m}$ in size (Ananyeva et al., 2013) were found to support SOC
70 protection. 30–150 μm pores are also the preferential places for new carbon inputs and greater abundance of such
71 pores translates into a higher spatial footprint that microbes make on SOC storage capacity (Kravchenko et al., 2019).
72 Therefore, the relationships between pore structure and SOC varied significantly under different soil conditions. Soils
73 in alpine ecosystems store large amounts of SOC and microorganisms habiting in alpine ecosystems were found to be
74 more tolerant to cold environments than those in other ecosystems (Zhao and Hu, 2023b). These results indicated that
75 relationships between pore structure and SOC fractions of alpine soils can be complex and are critical for
76 understanding the microscale mechanisms of the alpine carbon sinks. The dynamics of SOC during the FT process
77 could be significantly correlated with the transformation and destruction of aggregates (Dagesse, 2013). However, the
78 relationships between pore structure and SOC fractions are still not well understood for alpine soils under FT processes.

79 The Qinghai-Tibet Plateau (QTP) has the largest permafrost coverage in the middle to low latitudes of the world
80 (Wu et al., 2010). Soils of the QTP are fragile and vulnerable to environmental changes. Dramatic changes have
81 occurred in FT occurrence in recent years in the QTP as the depth and duration of FT processes have decreased while
82 the frequency of FT cycles has increased (Peng et al., 2017). Previous studies have demonstrated that FT cycles are
83 critical in influencing soil structure of the QTP (Gao et al., 2020; Yang et al., 2021). Alpine meadow soil
84 macroaggregates of the QTP had dense pore networks with many elongated pores in them due to frequent FT cycles
85 (Wang and Hu, 2023). FT processes led to opposite changes in the intra-aggregate porosity and interaggregate porosity
86 of alpine meadow soil (Zhao and Hu, 2022). Soils of the QTP serve as important SOC pools, and 36%-50% of the
87 SOC is concentrated in the 0-50 cm soil layer (Ding et al., 2016; Mu et al., 2020). Intensified FT cycles, especially
88 thawing processes, have led to large amounts of SOC loss, while the changes in SOC fractions remain unknown (Todd-
89 Brown et al., 2014; Liu et al., 2018). Liu et al. (2022) reported that topsoil POC content decreased upon permafrost
90 thawing, while MAOC content remained stable on the QTP. Deeper soil layers are more active in SOC changes as



91 these layers spend more time thawing (Chen et al., 2023). However, the responses of pore structure and SOC fractions
92 of aggregates to seasonal FT processes have been overlooked due to difficulties associated with monitoring on the
93 QTP, which has important implications for predicting carbon turnover projections under global warming (He et al.,
94 2021).

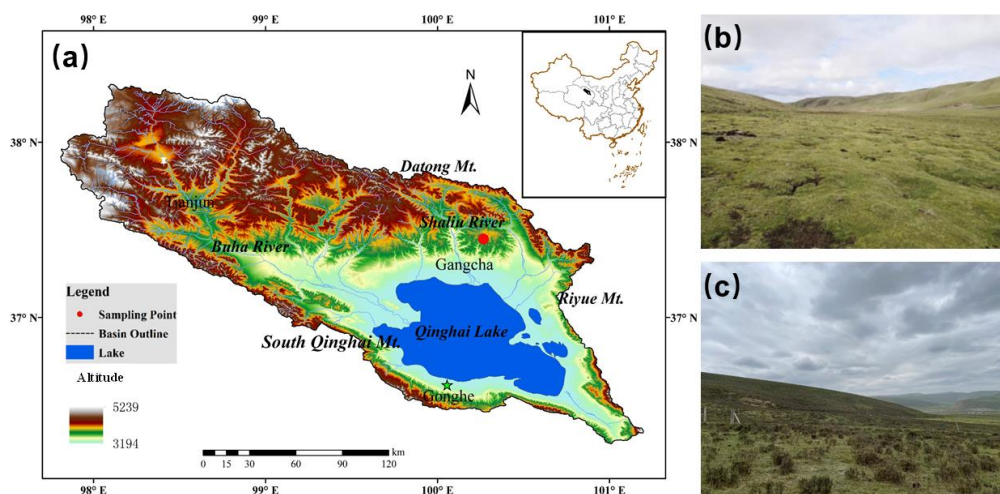
95 To fill these research gaps, the objectives of the study were: (1) to quantify changes in pore structure and the
96 SOC fraction content of aggregates in typical alpine ecosystems during the seasonal FT process; (2) to investigate the
97 relationships between them and (3) to clarify the role of pore structure on aggregate functions related to SOC
98 protection during seasonal freeze–thaw processes.

99 **2. Materials and methods**

100 *2.1 study sites and sampling*

101 The study was carried out in the Qinghai Lake Watershed (36°15'N-38°20'N, 97°50'-101°20'E), northeastern QTP.
102 The area lies in the cold and high-altitude climate zone, with a mean annual temperature and precipitation of 0.1 °C
103 and 400 mm, respectively (Li et al., 2018). Two ecosystems were selected in the study: *Kobresia pygmaea* meadow
104 (KPM) and *Potentilla fruticosa* shrubland (PFS). They are representative terrestrial ecosystems of the Qinghai Lake
105 watershed and account for over 60% of the watershed land area (Hu et al., 2016). One of the main features of these
106 two ecosystems is the mattic epipedon present on the soil surface. Mattic epipedon is the surface layer consisting of a
107 grass felt-like complex formed by the interweaving of live and dead roots of different ages. The layer is soft and
108 significantly affects SOC storage and soil structure (Hu et al., 2023). The soil type was classified as Gelic Cambisols
109 according to the FAO UNESCO system (IUSS Working Group WRB, 2022). We tried to avoid the simple pseudo
110 replication so that each sampling sites have a certain distance with others (> 1 km). Three sites within each ecosystem
111 have similar vegetation conditions. In every FT period, three sampling plots (1 m × 1 m) were set up at each site.

112



113

114 Fig. 1. Location of the sampling site (a) and landscapes of the (b) *Kobresia pygmaea* meadow ecosystem and (c)

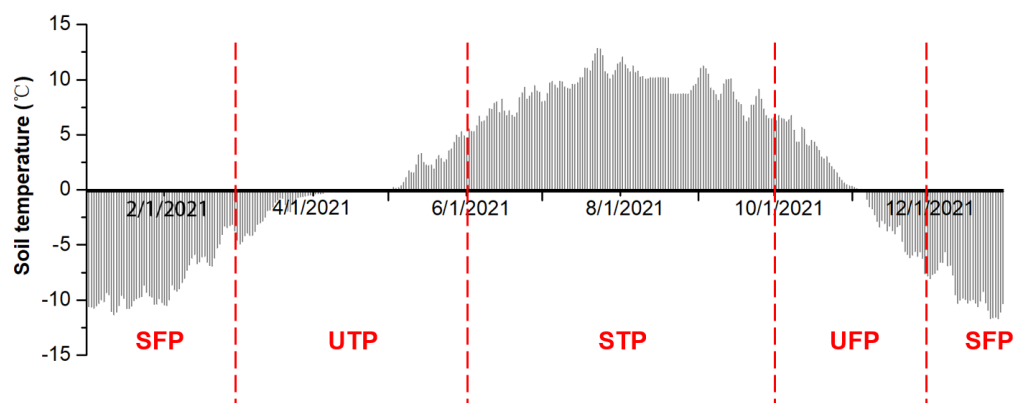
115

Potentilla fruticosa shrub ecosystem.

116

117 The division of seasonal FT periods is based on changes in daily soil temperature (Chen et al., 2021; Wu et al.,
118 2023). The EM-50 soil temperature data for 2019, 2020, and 2021 were obtained at 0.5 Hz with 30 min averages at
119 all three study sites using the ECH2O 5TE sensor (Decagon Devices, USA) (Li et al., 2018). The seasonal freeze–
120 thaw process was divided into four periods in this study: the unstable freezing period (UFP, as soil temperature starts
121 to drop to 0°C), the stable frozen period (SFP, with soil temperature completely below 0 °C), the unstable thawing
122 period (UTP, as soil temperature starts to rise above 0 °C), and the stable thawed period (STP, with soil temperature
123 completely above 0 °C). The freezing process included the SFP and UFP, while the thawing process included the STP
124 and UTP. Soil samples were taken in October 2021 (representing UFP), January 2022 (representing SFP), May 2022
125 (representing UFP) and July 2022 (representing SFP).

126



127
 128 Fig. 2. Daily average soil temperature in 2021 and the classification of freeze–thaw stages (SFP–stable frozen period,
 129 UTP–unstable thawing period, STP–stable thawing period and UFP–unstable freezing period).

130

131 In every site, soils samples from three soil profiles were dug for replicates. A total of 18 soil profiles were obtained
 132 in every FT period. We classified the soil layers as 0–10 cm, 10–30 cm and 30–50 cm soil layers. Soil cores and bulk
 133 soil were collected at each soil layer for aggregate sieving and physiochemical characteristic measurements,
 134 respectively. Soil cores were obtained using an 80 mm diameter soil auger and then preserved in an icebox before
 135 being sieved in the laboratory. A total of 54 soil cores were collected in every FT period. The basic soil properties of
 136 each soil layer at the study site are listed in Table S1. Particle size distribution was determined using the sieve-pipette
 137 method (Mako et al., 2019; Zhao et al., 2021). The soil water content as weight was determined using an oven-dried
 138 method (Klute, 1986). Soil pH measurements were conducted by an FE20 pH meter (Mettler Toledo, Columbus, USA)
 139 from slurries of samples at a soil:water ratio of 1:2.5 (w:w) (Zhao et al., 2020). SOC and TN were determined using
 140 a CN 802 elemental analyzer (VELP, Italy). Inorganic carbon was removed from the soil samples using 1 mol/L HCl
 141 prior to elemental analysis (Zhang et al., 2017).

142 2.2 Aggregate sieving

143 Separation of the soil aggregates was performed using the dry sieving method with 0.053, 0.25- and 2-mm sieves
 144 from top to bottom. Soil cores were gently broken by hand into 1-cm clods, and then soils were laid out between sheets
 145 of brown paper (Schutter and Dick, 2002). Debris such as gravel and roots were removed from the samples. Two
 146 hundred grams of soil was placed on the top sieve and was shaken for five minutes by the sieve shaker. Therefore, the
 147 aggregates were divided into four categories: large macroaggregates (LMAs, with diameters >2 mm), small
 148 macroaggregates (SMAs, with diameters of 0.25–2 mm), microaggregates (mAs, with diameters of 0.053–0.25 mm),
 149 and fractions with diameters <0.053 mm. aggregate fractions of LMAs and SMAs were weighed and preserved for

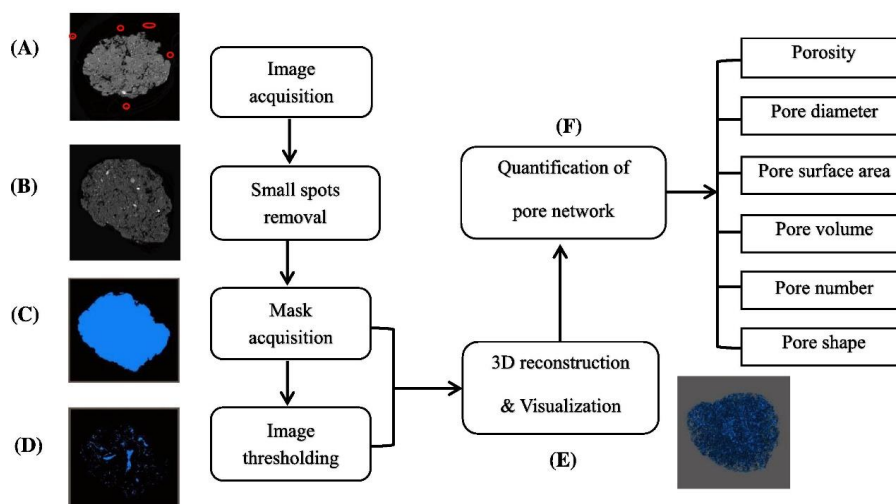


150 further analysis.

151 *2.3 CT scanning and image processing*

152 A nanoVoxel-4000 X-ray three-dimensional microscopic CT (Sanying Precision Instruments Co., Ltd., China)
 153 was used to scan the soil aggregates with X-ray source parameters of voltage 80 kV and current 50 μ A, with which
 154 2800 detailed and low-noise images could be obtained during a 360° rotation. The reconstructed images featured a 3.6
 155 μ m spatial resolution and 2800 \times 2800 \times 1500 voxels. Aggregate fractions of > 2 mm and 0.25-2 mm from all soil
 156 layers of the UFP, SFP, UTP and STP periods were scanned (other fractions were too small to separate into a single
 157 sample).

158 Reconstruction of the pore network of aggregates was completed using Avizo 9.0 (Visualization Sciences Group,
 159 Burlington, MA). The procedure for image analysis was similar to that described by Wang and Hu (2023) (Fig. 3).
 160 Briefly, the clutters around the aggregates were eliminated using a volume-editing module. Mask extraction was
 161 carried out in the segmentation module (Zhao et al. 2020). The soil matrix was selected with the “Magic Wand” tool,
 162 and then the “Fill” tool was used to fill the pores for obtaining the aggregate boundary and the mask of the whole
 163 aggregate (Zhao and Hu, 2023a). All images were binarily segmented using the histogram thresholding method based
 164 on the global thresholding algorithm (Jaques et al., 2021), and pore thresholds were selected for all images.



165

166 Fig. 3. Procedures used for the visualization and quantification of soil aggregate pore networks. Taken from Zhao et

167

al. (2020) with permission from Elsevier.

168

169 The two-dimensional images were transformed into 3D images by Volume Rendering tool in Avizo 9.0 software.



170 The intra-aggregate porosity was calculated using the Volume Fraction tool. The Volume Rendering tool transferred
171 the 2D images into 3D images before the equivalent diameter, volume, number, length, and surface area were
172 calculated using the Label Analysis tool. The pore number density (ND) is defined as the ratio of the pore number (n)
173 to the total volume of the aggregate samples (V):

$$174 \quad ND = \frac{n}{V} \quad (1)$$

175 One pore network may consist of several branches of connected pores or just one individual pore. The pore length
176 is the total actual length in all branches. The pore length density (LD) is defined as the ratio of the pore length (L) to
177 the total volume of pores (V) (Yang et al., 2021):

$$178 \quad LD = \frac{L}{V} \quad (2)$$

179 The surface area density (SD) is defined as the ratio of the pore surface area (S) to the total volume of V:

$$180 \quad SD = \frac{S}{V} \quad (3)$$

181 To characterize the pore shape, the pore shape factor (SF) was calculated as follows:

$$182 \quad SF = \frac{A_0}{A} \quad (4)$$

183 where A_0 represents the surface area of the equivalent sphere of the pores and A is the actual surface area of
184 the pores. SF values closer to 1 indicate a more regular pore shape (i.e., closer to a spherical shape), and smaller values
185 refer to more irregular or elongated pore shapes (Zhou et al., 2012).

186 The equivalent diameter (EqD) was defined as the diameter of spherical particle with the same volume and was
187 calculated by pore volume:

$$188 \quad EqD = \sqrt[3]{\frac{6 \times V}{\pi}} \quad (5)$$

189 Where V represents the volume of pores.

190 The pores were divided into four classes based on their equivalent diameter: <15, 15–30, 30–80, and >80 μm .
191 According to Lal and Shukla (2004), pores <30, 30–80, and >80 μm are termed micropores, mesopores and
192 macropores, respectively.

193 2.4 SOC fraction separation

194 In every FT period, macroaggregate samples were sufficiently ground to pass through a 0.15 mm sieve before
195 their total organic carbon content (TOC) content was measured using the CN 802 elemental analyzer (VELP, Italy).

196 The determination of SOC fractions, including POC and MAOC, was performed as described by Cambardella



197 and Elliott (1992). Approximately 5 g of each dried aggregate of the LMA and SMA fractions was moved to a 50 mL
198 centrifuge tube and dispersed in 25 mL of a sodium hexametaphosphate (0.5%, w/v) solution by shaking for 18 h in a
199 reciprocating shaker at 120 RMP to ensure that it was evenly blended. The dispersed samples were rinsed onto a 53
200 μm sieve to separate MAOC (particle size $<53 \mu\text{m}$) and POC (particle size $>53 \mu\text{m}$) using distilled water until the
201 water stream was clear and free of fine soil particles. After that, samples were transferred to evaporating dishes and
202 dried at 65 °C for 48 h to isolate soils which contained POC or MAOC fractions solely (Six et al., 1998). After
203 weighing and sieving, all the fractions' SOC contents were measured using the CN800 elemental analyzer. The POC
204 and MAOC contents were obtained by multiplying the percentage of each particle size fraction in the soil (Sun et al.,
205 2023).

206 2.5 Statistical analysis

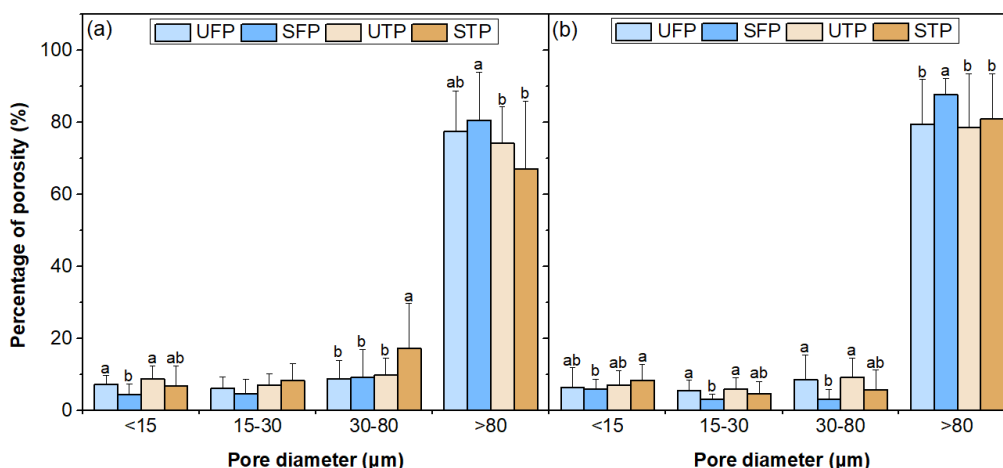
207 All statistical analyses except redundancy analysis (RDA) were conducted with IBM's SPSS 20 software (SPSS
208 Inc., USA). One-way analysis of variance (ANOVA) was conducted to compare differences between the four seasonal
209 freezing-thawing stages and different aggregate fractions. Pearson's correlations were conducted to evaluate the
210 linkages between pore characteristics and SOC fractions of macroaggregates. RDA was conducted to determine pore
211 parameters that had a significant impact on SOC fractions and was carried out in R software (<http://www.r-project.org>)
212 using the vegan package.

213 3. Results

214 3.1 Soil pore characteristics of aggregates

215 Fig. 4 depicts the pore size distribution of soil aggregates during the seasonal FT process. In the two ecosystems,
216 pores of $> 80 \mu\text{m}$ dominated the pore space in all periods and accounted for over 65% of the total porosity. The
217 contribution of pores of $< 15 \mu\text{m}$ was low in the stable frozen period with 4.39 % in the meadow ecosystem and 5.36 %
218 in the shrubland ecosystem. The volume percentage of pores of $> 80 \mu\text{m}$ was high in the stable frozen period (80.62%
219 in the meadow ecosystem and 87.65% in the shrubland ecosystem) and was significantly higher than that in the UTP
220 (74.17% in the meadow ecosystem and 78.53% in the shrubland ecosystem) and the STP (67.18% in the meadow
221 ecosystem and 80.96% in the shrubland ecosystem) ($P<0.05$). The results showed that freezing process enhanced the
222 formation of pores of $> 80 \mu\text{m}$.

223



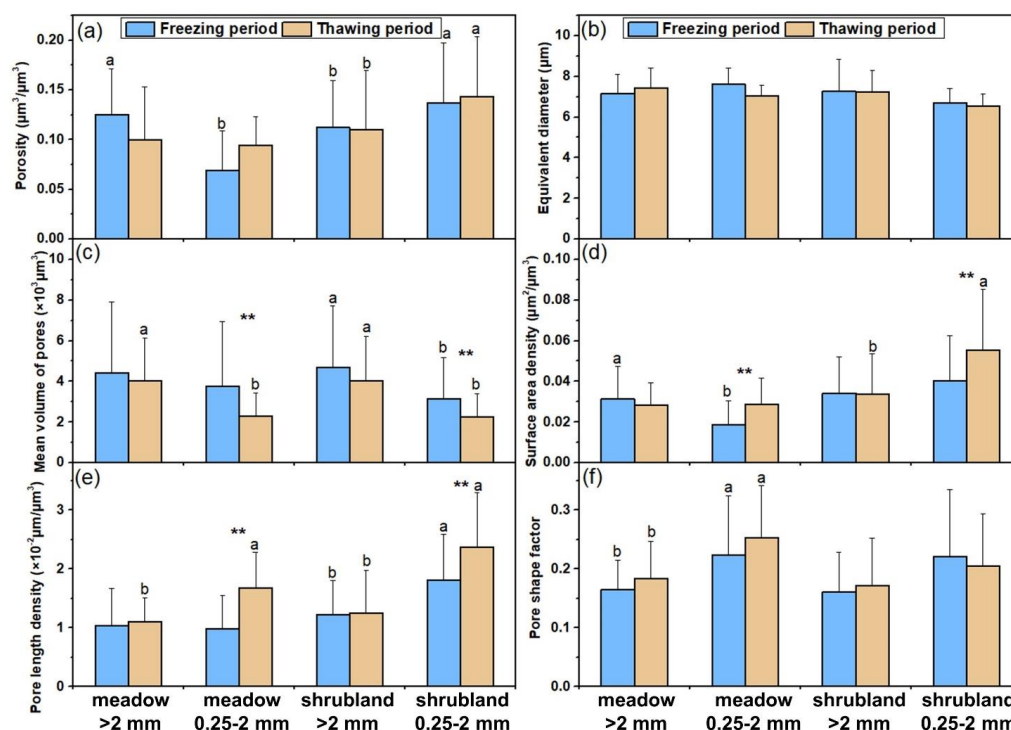
224

225 Fig. 4. Pore size distribution (by pore diameter) of soil aggregates in the (a) meadow ecosystem and (b) shrubland
 226 ecosystem during the seasonal FT process. Bars represent the mean \pm standard error (n=18). Different lowercase letters
 227 denote significant differences among pore volume percentages in different FT periods ($P < 0.05$).

228 Note: UFP-unstable freezing period, SFP-stable frozen period, UTP-unstable thawing period, STP-stable thawed
 229 period.

230 The characteristics of the pores of aggregates during the seasonal FT process are shown in Fig. 5. The seasonal
 231 FT process did not significantly affect the EqD (Fig. 5b). The mean pore volumes of 0.25-2 mm aggregates in the
 232 freezing period ($3.76 \times 10^3 \mu\text{m}^3$ and $3.14 \times 10^3 \mu\text{m}^3$ in the meadow and shrubland ecosystems respectively) were
 233 significantly higher than those in the thawing period ($2.30 \times 10^3 \mu\text{m}^3$ and $2.24 \times 10^3 \mu\text{m}^3$ in the meadow and shrubland
 234 ecosystems respectively), while no significant difference was observed for > 2 mm aggregates (Fig. 5c). In the meadow
 235 ecosystem, the pore length density of the 0.25-2 mm aggregates was $1.68 \times 10^{-4} \mu\text{m} \mu\text{m}^{-3}$ in thawing period, which was
 236 1.71 times higher than that in the freezing period ($0.98 \times 10^{-4} \mu\text{m} \mu\text{m}^{-3}$). In the shrubland ecosystem, pore surface area
 237 density and length density of 0.25-2 mm aggregates were $0.0553 \mu\text{m}^2 \mu\text{m}^{-3}$ and $2.37 \times 10^{-4} \mu\text{m} \mu\text{m}^{-3}$, respectively, both
 238 significantly higher than those in the freezing period ($0.0404 \mu\text{m}^2 \mu\text{m}^{-3}$ and $1.81 \times 10^{-4} \mu\text{m} \mu\text{m}^{-3}$ for surface area density
 239 and length density, respectively). Therefore, seasonal FT processes mainly led to changes in the pore characteristics
 240 of 0.25-2 mm aggregates rather than those of > 2 mm aggregates.

241 In the meadow ecosystem, the SF of pores of the 0.25-2 mm aggregates (0.224 in the freezing period and 0.253
 242 in the thawing period) exceeded those of > 2 mm aggregates (0.164 in the freezing period and 0.184 in the thawing
 243 period), while no significant difference in SF was found in the shrubland ecosystem (Fig. 5f).

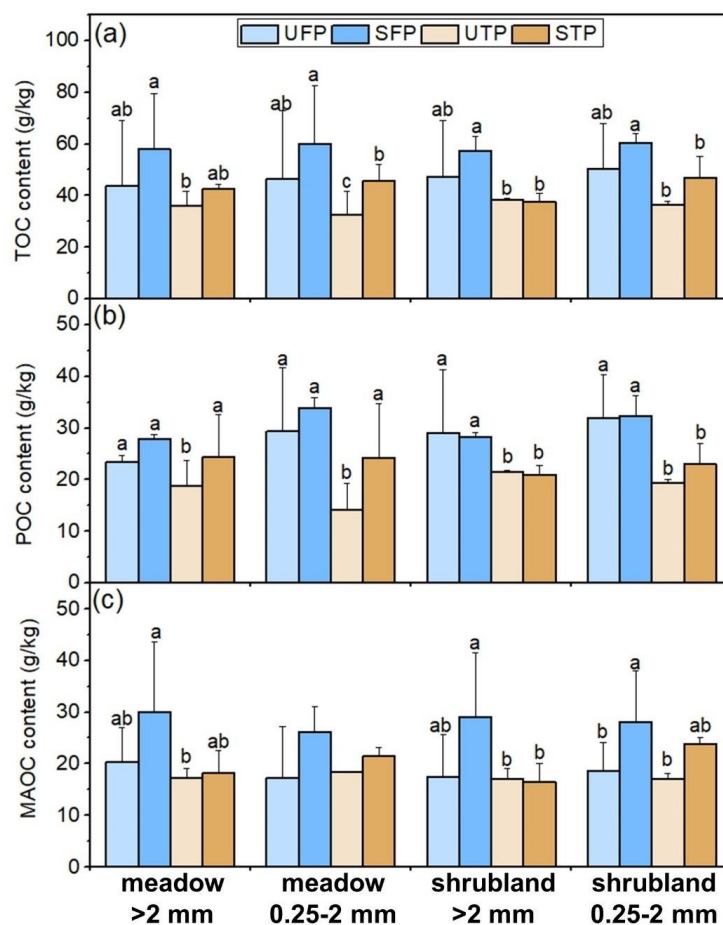


244

245 Fig. 5. Pore characteristics of soil aggregates during the seasonal FT process. (a) porosity, (b) pore equivalent diameter,
 246 (c) mean volume of pores, (d) pore surface area density, (e) pore length density and (f) pore shape factor. Bars represent
 247 the mean \pm standard error (n=9). ** represents significant differences between pore characteristics in freezing period
 248 and thawing period ($P < 0.05$). Different lowercase letters denote significant differences between pore characteristics
 249 of > 2 mm aggregates and 0.25-2 mm aggregates ($P < 0.05$).

250 *3.2 SOC fraction contents of aggregates*

251 The SOC fraction contents (TOC, POC and MAOC) of aggregates during seasonal freeze–thaw process are
 252 shown in Fig. 6. Generally, in the two ecosystems, the TOC contents of aggregates peaked in the stable frozen period,
 253 ranging from 57.33 g/kg to 60.28 g/kg (Fig. 6a). The following unstable thawing period demonstrated the significant
 254 decline in TOC contents of > 2 mm (dropped by 37.73% and 32.95% in the meadow and shrubland ecosystems,
 255 respectively) and 0.25-2 mm aggregates (dropped by 45.57% and 39.43% in the meadow and shrubland ecosystems,
 256 respectively) ($P < 0.05$). In the shrubland ecosystem, TOC contents of aggregates in the stable thawed period were also
 257 significantly lower than those in the stable frozen period ($P < 0.05$).



258

259 Fig. 6. Changes of SOC content (a-TOC, b-POC and c-MAOC) of soil aggregates during the seasonal freeze–thaw
 260 process. Bars represent the mean ± standard error (n=9). Different lowercase letters denote significant differences
 261 among SOC contents in different FT periods (P<0.05).

262 Note: UFP-unstable freezing period, SFP-stable frozen period, UTP-unstable thawing period, STP-stable thawed
 263 period.

264 Changes in contents of POC and MAOC were similar to those of TOC (Fig. 6b and 6c). In the meadow ecosystem,
 265 the POC contents were high in the stable frozen period (27.90 g/kg for > 2 mm aggregates and 33.77 g/kg for 0.25-2
 266 mm aggregates) and the POC contents in the unstable thawing period (18.78 g/kg for > 2 mm aggregates and 14.18
 267 g/kg for 0.25-2 mm aggregates) were significantly lower than those in other periods (P<0.05) (Fig. 6b). The MAOC
 268 content of > 2 mm aggregates was 29.99 g/kg in the stable frozen period, which was 1.74 times higher than that in the



269 unstable thawing periods (17.28 g/kg) (Fig. 6c). In the shrubland ecosystem, POC contents in freezing periods were
 270 significantly higher than those in thawing periods ($P < 0.05$) (Fig. 6b). The unstable thawing process led to significant
 271 loss in MAOC compared with the stable freezing period (41.54% for POC and 39.14%) ($P < 0.05$) (Fig. 6c).

272 The changes in the coefficient of variation (CV) during the seasonal FT process, which depicted the variation in
 273 the SOC content of aggregates from different soil depths, were shown in Table 1. In the two ecosystems, the CV values
 274 in the stable frozen period (0.20 for the meadow ecosystem and 0.22 for the shrubland ecosystem) were significantly
 275 lower than those in other periods ($P < 0.05$). These results revealed that freezing resulted in a more uniform distribution
 276 of SOC across different soil layers.

277 Table 1 Coefficient of variation (CV) of SOC content of aggregates in all soil layers during the seasonal FT process.

Ecosystem	Seasonal FT periods			
	UFP	SFP	UTP	STP
meadow	0.38a	0.20b	0.47a	0.56a
shrubland	0.46a	0.22b	0.34a	0.34a

278 Note: UFP-unstable freezing period, SFP-stable frozen period, UTP-unstable thawing period, STP-stable thawed
 279 period. Different lowercase letters denote significant differences in CV of different FT periods.

280 3.3 Relationships between pore structure and SOC fractions of aggregates

281 Tables 2 demonstrates the relationships between pore structure and SOC fractions of aggregates in the freezing
 282 process (UFP and SFP) and thawing process (UTP and STP). In the freezing process, the POC content was positively
 283 correlated with pores of $< 15 \mu\text{m}$ ($P < 0.05$). The TOC and MAOC contents were both positively correlated with pore
 284 length density ($P < 0.05$). In the thawing process, no correlations were observed between SOC fractions and pore
 285 parameters while pore size distribution had significant impact on SOC content. The TOC and MAOC contents were
 286 both positively correlated with pores of $< 15 \mu\text{m}$ and of $> 80 \mu\text{m}$ ($P < 0.05$) but negatively correlated with pores of 15-
 287 $30 \mu\text{m}$ ($P < 0.05$).

288 RDA was used to explain the relationship between the pore parameters and SOC fractions during the seasonal
 289 FT process (Fig. 7). In the freezing period, a total of 53.29% of the SOC variation could be explained by pore
 290 characteristics (Fig. 7a). Pore equivalent diameter had a significant impact on SOC content ($P < 0.05$). In thawing
 291 period, 52.90% of the SOC variation, with 50.99% on Axis 1 and 1.91% on Axis 2, was explained by pore
 292 characteristics (Fig. 7b). Pore surface area and EqD played important roles in SOC dynamics of aggregates ($P < 0.05$).



293

Table 2 Correlations between SOC content, soil microbial characteristics and soil structure of soil aggregates in freezing period and thawing period

	Freezing period									
	Equivalent diameter	Mean volume	Pore surface area density	Pore length density	Pore shape factor	Pd<15	Pd15-30	Pd30-80	Pd>80	
TOC	0.428	-0.404	-0.124	0.553	0.718*	0.241	0.420	0.084	0.316	-0.235
POC	0.222	-0.252	0.188	0.339	0.397	0.032	0.639*	0.123	0.410	-0.273
MAOC	0.529	-0.443	-0.479	0.622*	0.865**	0.422	0.013	0.010	0.086	-0.106

	Thawing period									
	Equivalent diameter	Mean volume	Pore surface area density	Pore length density	Pore shape factor	Pd<15	Pd15-30	Pd30-80	Pd>80	
TOC	0.582	-0.507	-0.036	0.326	0.396	0.199	0.811*	-0.834**	-0.503	0.733*
POC	0.521	-0.214	-0.274	0.178	0.428	0.538	0.458	-0.353	-0.146	0.295
MAOC	0.409	-0.498	0.117	0.296	0.234	0.071	0.727*	-0.818*	-0.532	0.727*

294 Note: * represents the correlation is significant (P<0.05), Pd<15: volume percentage of pores <15 µm, Pd15-30: volume percentage of pores 15-30 µm; Pd30-80: volume percentage
 295 of pores 30-80 µm; Pd>80: volume percentage of pores >80 µm.

296

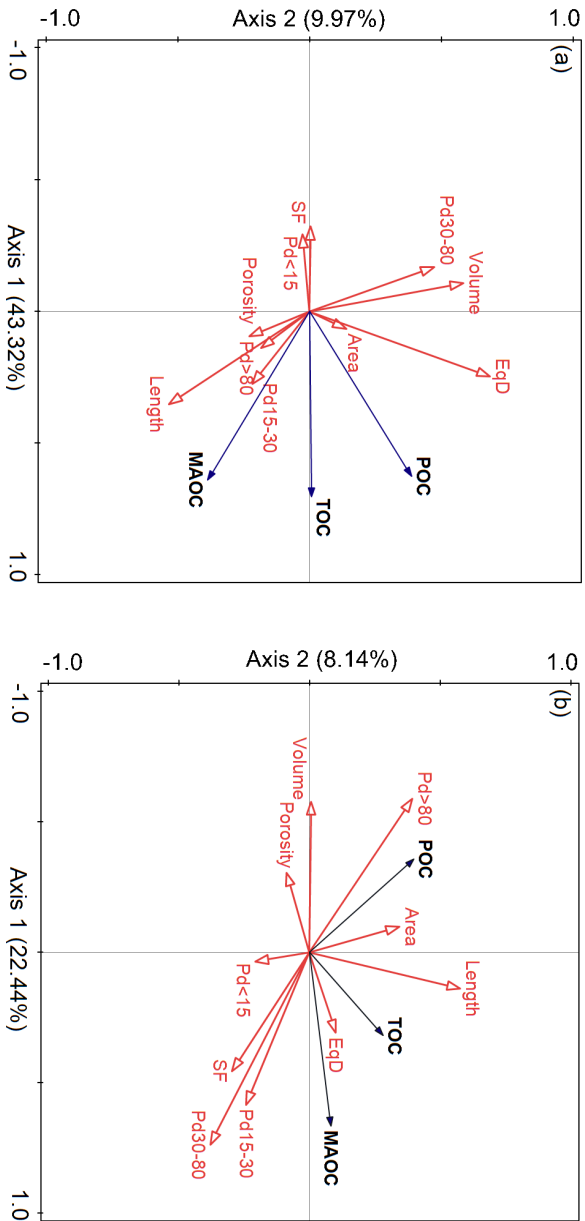


Fig. 7. RDA analysis between SOC content and pore characteristics of aggregates in (a) the freezing period and (b) the thawing period.

297
298
299 Note: Volume-pore volume, EqD-equivalent diameter of pores, Pd30-80-pores with diameter of 30-80 μm , SF-pore shape factor, Pd<15: pores with diameter of <15 μm , Pd15-30-
300 pores with diameter of 15-30 μm , Pd>80- pores with diameter of > 80 μm .



301 **4. Discussion**

302 Our results demonstrated that the volume percentage of aggregates was high in the stable frozen period. This
303 finding is consistent with previous results, which showed that FTCs resulted in an increase in macroporosity, with a
304 significant increase observed after the 3rd FTC compared to no FT control (Wu and Hu, 2024). The impact of seasonal
305 FT processes on aggregate pore structures is similar to the those of simulated FT cycles. The FT processes initially
306 altered soil pore network due to frost heave and reorganization of particles (Zhang et al., 2016). These changes
307 therefore drive soil development processes (Ping et al., 2015). Ma et al. (2020) found volume percentage of pores of >
308 100 μm in aggregates increased from 62.39% to 96.53% after 20 times FT cycles. During the freezing process, pore-
309 scale heterogeneities cause pressure gradients and the seepage of water from smaller to larger pores (Rempel and van
310 Alst, 2013), and this process enhance the expansion of force heave (Skvortsova et al., 2018). Freezing could also
311 increase pore size by forming new connections among adjacent pores (Ma et al., 2020). The increase in pore size and
312 porosity could loosen the aggregate stability and increase pore air content, thus increasing the air pressure and
313 enhancing expansion (Lugato et al., 2010; de Jesus Arrieta Baldovino et al., 2021). We also found that the seasonal
314 FT process mainly affects the pore characteristics of 0.25-2 mm aggregates rather than those of > 2 mm aggregates,
315 especially in the pore surface area density and length density. Zhao and Hu (2023a) reported a similar significant
316 change in pore surface area density of 0.25-1 mm aggregates after FT cycles. Changes in surface area density and pore
317 length density or pores might be associated with pore shape (Rooney et al., 2022). In the freezing period, the frost
318 heave force of water is anisotropic, which increases the pore length and decreases the surface area. In summary,
319 freezing increased the pore volume and the impact of seasonal FT processes on pore characteristics is dependent on
320 aggregate size.

321 Our results revealed that the contents of SOC fractions were all high in the stable frozen period and low in the
322 unstable thawing period, which is similar to previous findings. Huang et al. (2021) found that the TOC content of
323 aggregates was high in January and February and showed a significant decrease in March due to FT processes. Many
324 studies have also reported the SOC loss at the beginning of the thawing period at regional scales (Song et al., 2014;
325 Song et al., 2020). This phenomenon can be explained by litter accumulation and suppressed microbial activities in
326 freezing periods (Han et al., 2018), as well as the aerobic environment intensifying SOC mineralization during thawing
327 (Liu et al., 2018; Liu et al., 2021). Additionally, in these two ecosystems, a large amount of plant litter accumulated
328 and transformed into substrates in the freezing period and served as important source of SOC. This phenomenon may
329 have occurred because soil aggregates are sensitive to physical disruption, and FTCs affect the stability of aggregates,
330 leading to a release of POC and MAOC that is trapped within aggregates by physical occlusion and facilitating



331 organic-mineral bonding between clay and microbial residues (Bailey et al., 2019; Six et al., 2004). So, the freezing
332 process promoted SOC accumulation while the thawing process induced a loss of SOC.

333 The results revealed that pore equivalent diameter explained most in the SOC variations. In the freezing process,
334 pores of $< 15 \mu\text{m}$ served as preferential spots for POC stabilization. As the period is featured by SOC accumulation,
335 $< 15 \mu\text{m}$ pores reduced SOC decomposition via limiting microbial access, gas diffusion and water availability, shifting
336 microbial metabolism to less efficient anaerobic respiration (Strong et al., 2004; Keiluweit et al., 2017; Wang and Hu,
337 2023). In the thawing period, the TOC and MAOC contents were both positively correlated with pores of $> 80 \mu\text{m}$
338 and negatively correlated with pores of $15\text{-}30 \mu\text{m}$. Pores of $> 80 \mu\text{m}$ serve as primary sites for residue entry and are
339 promoted by microbial materials and SOC, which enhance soil aggregation and thus drive more SOC to be protected
340 (Ananyeva et al., 2013; Dal Ferro et al., 2014; Zhang et al., 2023). Pores of $15\text{-}30 \mu\text{m}$, on the other side, might have
341 negative impact on SOC protection (Liang et al., 2019). These pores are accompanied by enhanced microbial activities
342 led to the mineralization of greater amounts of SOC (Kravchenko et al., 2015; Zhang et al., 2023). In summary,
343 considering the dramatic change in porosity of $<15 \mu\text{m}$ and $>80 \mu\text{m}$ pores, the seasonal FT process altered the SOC
344 protection of aggregates via regulating pore size distribution.

345 In this study, we explored changes in the pore structure and SOC fractions of alpine soil macroaggregates in the
346 seasonal FT process. However, we could not isolate the impact of FT processes on soil structure and functions as
347 impacts from vegetation and climate could not be avoided under field conditions. Therefore, it is necessary to compare
348 the results based on indoor FT simulations and field sampling in future studies to clarify the importance of FT
349 processes in shaping pore structure and affecting soil functions. Recent studies have clarified the importance of
350 minerals (e.g., Fe, Al, and their oxides) in microscale SOC protection (Kang et al., 2024; Wang et al., 2024; Zhu et al.,
351 2024). Establishing relationships between structural characteristics and minerals can help us better understand the role
352 of pore structure in SOC protection mechanisms.

353 5. Conclusion

354 The findings of the study revealed that seasonal freeze–thaw processes regulate pore structure, and SOC
355 concentration of aggregates. The seasonal FT process significantly affected the pore surface area density and length
356 density of $0.25\text{-}2 \text{ mm}$ aggregates. The freezing process promoted the formation of pores $> 80 \mu\text{m}$ while thawing led
357 to shrinkage of pore space. Freezing enhanced the accumulation of SOC of aggregates and the more uniform
358 distribution of SOC among different soil layers. Thawing processes witnessed the loss of SOC. The seasonal FT
359 process altered the SOC protection of aggregates via regulating pore size distribution. In the freezing process, pores
360 of $< 15 \mu\text{m}$ enhanced the protection of SOC of aggregates by limiting microbial access and shaping anerobic



361 environments. In the thawing process, pores of 15-30 μm contributed to the SOC loss. Overall, our study explains the
362 changes in SOC during the freeze-thaw process by innovatively establishing a pathway of FT-pore structure-SOC.
363 This study has critical implications for predicting soil structural dynamics and reducing uncertainty in global carbon
364 cycle predictions under climate change.

365 **Abbreviations**

366 FT: freeze-thaw, FTC: freeze-thaw cycle, UFP: unstable freezing period, SFP: stable frozen period, UTP:
367 unstable thawing period, STP: stable thawed period, EqD: equivalent diameter of pores, SF: shape factor, LMA: large
368 macroaggregate, SMA: small macroaggregate, SOC: soil organic carbon, TOC: total organic carbon, POC: particulate
369 organic carbon, MAOC: mineral-associated organic carbon.

370 **Declarations**

371 **Acknowledgement**

372 This study was financially supported by the National Science Foundation of China (Grant number: 42371107)
373 and the Project Supported by State Key Laboratory of Earth Surface Processes and Resource Ecology (2022-TS-03).

374 **CRediT authorship contribution statement**

375 Ruizhe-Wang: Conceptualization; data curation; formal analysis; methodology; writing-original draft; writing-
376 review & editing. Xia Hu: Funding acquisition; investigation; project administration; supervision; writing-review &
377 editing.

378 **Availability of data and material**

379 All data generated or analyzed during this study are included in this published article [and its supplementary
380 information files.

381 **Declaration of competing interests**

382 The authors declare that they have no known competing financial interests or personal relationships that could
383 have appeared to influence the work reported in this paper.

384



385 **References**

- 386 Ananyeva, K., Wang, W., Smucker, A.J.M., Rivers, M.L., Kravchenko, A.N., Can intra-aggregate pore structures affect
387 the aggregate's effectiveness in protecting carbon? *Soil Bio. Biochem.* 57, 868–875. doi:
388 10.1016/j.soilbio.2012.10.019, 2013.
- 389
- 390 Angassa, A. Effects of grazing intensity and bush encroachment on herbaceous on species and rangeland condition
391 in southern Ethiopia. *Land Degradation Development*, 25: 438.451. doi: 10.1002/ldr.2160, 2014.
- 392
- 393 Bronick, C.J., Lal, R. Soil Structure and management: a review. *Geoderma* 124, 3–22. doi:
394 10.1016/j.geoderma.2004.03.005, 2004.
- 395
- 396 Cambardella, C.A., Elliott, E.T. Particulate soil organic-matter changes across a grassland cultivation sequence. *Soil
397 Science Society of American Journal* 56(3): 777-783. doi: 10.2136/sssaj1992.03615995005600030017x, 1992.
- 398
- 399 Campbell, J.L., Soggi, A.M., Templer, P.H. Increased nitrogen leaching following soil freezing is due to decreased
400 root uptake in a northern hardwood forest. *Global Change Biology* 20, 2663–2673. doi: 10.1111.gcb.12532.
401 2014.
- 402
- 403 Chen, H., Huang, Y., He, K., Qi, Y., Li, E., Jiang, Z., Sheng, Z., Li, X. Temporal intraspecific trait variability drives
404 responses of functional diversity to interannual aridity variation in grasslands. *Ecology and Evolution*, 9 (10),
405 5731-5742. doi: 10.1002/ece3.5156, 2019.
- 406
- 407 Chen, H., Liu, X., Xue, D., Zhu, D., Zhan, W., Li, W., Wu, N., Yang, G. Methane emissions during different
408 freezing-thawing periods from a fen on the Qinghai-Tibet Plateau: Four years of measurements. *Agricultural
409 and Forest Meteorology* 297, 108279. doi: 10.1016/j.agrformet.2020.108279. 2020.
- 410
- 411 Chen, L., Fang, K., Wei, B. Soil carbon persistence governed by plant input and mineral protection at the regional and
412 global scales. *Ecology Letters*, 24: 1018-1028. doi: 10.1111/ele.13883, 2021.
- 413



- 414 Chen, Y., Han, M., Yuan, X., Zhou, H., Zhao, x., Schimel, J.P., Zhu, B. Long-term warming reduces surface soil
415 organic carbon by reducing mineral-associated carbon rather than “free” particulate carbon. *Soil Biology and*
416 *Biochemistry* 177, 108905. doi: 10.1016/j.soilbio.2022.108905, 2023.
- 417
- 418 Dagesse, D.F. Freezing cycle effects on water stability of soil aggregates. *Canadian Journal of Soil Science* 93(4):
419 473-483. doi: 10.4141/CJSS2012-046, 2002.
- 420
- 421 Dal Ferro, N., Sartori, L., Simonetti, G., Berti, A., Morari, F. Soil macro-and microstructure as affected by different
422 tillage systems and their effects on maize root growth. *Soil and Tillage Research*, 140, 55–65. doi:
423 10.1016/j.still.2014.02.003, 2014.
- 424
- 425 de Jesus Arrieta Baldovino, J., dos Santos Izzo, R.L., Rose, J.L. Effects of freeze-thaw cycles and porosity/cement
426 index on durability, strength and capillary rise of a stabilized silty soil under optimal compaction conditions.
427 *Geotechnical and Geological Engineering* 39, 481-498. doi: 10.1007/s10706-020-01507-y. 2021.
- 428
- 429 Ding J., Chen, L., Zhang, B. Linking temperature sensitivity of soil CO₂ release to substrate, environmental, and
430 microbial properties across alpine ecosystems. *Global Biogeochemistry Cycles*, 30 (9), 1310-1323. doi:
431 10.1002/2015gb005333, 2016.
- 432
- 433 Gao, Z., Hu, X., Li, X., Li, Z. Effects of freeze–thaw cycles on soil macropores and its implications on formation of
434 hummocks in alpine meadows in the Qinghai Lake watershed, northeastern Qinghai-Tibet Plateau. *Journal of*
435 *Soils and Sediments*, 21:245-256. doi: 10.1007/s11368-020-02765-2, 2021.
- 436
- 437 Han, C., Gu, Y., Kong, M., Hu, L., Jia, Y., Li, F., Sun, G., Siddique, K.H.M. Responses of soil microorganisms,
438 carbon and nitrogen to freeze-thaw cycles in diverse land-use types. *Applied Soil Ecology*, 124: 211-217. doi:
439 10.1016/j.apsoil.2017.11.012, 2018.
- 440
- 441 He, L., Lai, C., Mayes, M.A., Murayama, S., Xu, X. Microbial seasonality promotes soil respiratory carbon
442 emission in natural ecosystems: a modeling study. *Global Change Biology*, 27, 3035–3051. doi:
443 10.1111/gcb.15627, 2021.



- 444
- 445 Hu, X., Li, Z., Li, X., Liu, L. Quantification of soil macropores under alpine vegetation using computed tomography
446 in the Qinghai Lake Watershed, NE Qinghai-Tibet Plateau. *Geoderma* 264, 244–251. doi:
447 10.1016/j.geoderma.2015.11.001, 2016.
- 448
- 449 Huang, D., Zhou, L., Fan, H., Jia, Y., Liu, M. Responses of aggregates and associated soil available phosphorus, and
450 soil organic matter in different slope aspects, to seasonal freeze–thaw cycles in Northeast China. *Geoderma*, 402,
451 115184. doi: 10.1016/j.geoderma.2021.115184, 2021.
- 452
- 453 IUSS Working Group WRB. World Reference Base for Soil Resources. International soil classification system for
454 naming soils and creating legends for soil maps, 4th ed. International Union of Soil Sciences (IUSS), Vienna,
455 Austria, 2022.
- 456
- 457 Jaques, V.A.J., Du Plessis, A., Zemek, M., Salplachta, J., Stubianova, Z., Zikmund, T., Kaiser, J. Review of porosity
458 uncertainty estimation methods in computed tomography dataset. *Measurement Science and Technology* 32, 12,
459 122001. doi: 10.1088/1361-6501/ac1b40, 2021.
- 460
- 461 Kallenbach, C.M., Frey, S.D., Grandy, A.S., Direct evidence for microbial-derived soil organic matter formation and
462 its ecophysiological controls. *Nature Communications* 7 (1), 1–10. Doi: 10.1038/ncomms13630, 2016.
- 463
- 464 Kang, J., Qu, C., Chen, W., Cai, P., Chen, C., Huang, Q. Organo-organic interactions dominantly drive soil organic
465 carbon accrual. *Global Change Biology* 30 (1): e17147. doi: 10.1111/gcb.17147, 2024.
- 466
- 467 Klute, A. *Methods of Soil Analysis: Part 1–Physical and Mineralogical Methods*. American Society of Agronomy,
468 Madison. 1986.
- 469
- 470 Kravchenko, A.N., Guber, A.K. Soil pores and their contributions to soil carbon processes. *Geoderma*. 287, 31–39.
471 doi: 10.1016/j.geoderma.2016.06.027, 2017.
- 472



- 473 Kravchenko, A.N., Guber, A.K., Razavi, B.S., Koestel, J.K., Quigley, M.Y., Robertson, G.P., Kuzyakov, Y., 2019.
474 Microbial spatial footprint as a driver of soil carbon stabilization. *Nature Communications*, 10: 3121.
475 <https://doi.org/10.1038/s41467-019-11057-4>.
476
477 Kravchenko, A.N., Negassa, W.C., Guber, A.K., Rivers, M.L. Protection of soil carbon within macro-aggregates
478 depends on intra-aggregate pore characteristics. *Scientific Reports*, 5 (1), 1–10. doi: 10.1038/srep16261, 2015.
479
480 Kreyling, J., Beierkuhnlein, C., Pirtsch, K., Schloter, M., Jentsch, A. Recurrent soil freeze–thaw cycles enhance
481 grassland productivity. *New Phytologist* Foundation 177:938–945. doi: 10.1111/j.1469-8137.2007.02309.x,
482 2017.
483
484 Lal, R., Shukla, M.K. *Principles of Soil physics*. Marcel Dekker, New York, 2004.
485
486 Lavallee, J.M., Soong, J.L., Cotrufo, M.F. Conceptualizing soil organic matter into particulate and mineral-associated
487 forms to address global change in the 21st century. *Global Change Biology*, 26(1). doi: 10.1111/gc.14859,
488 2020.
489
490 Lemanski, K., Armbruster, M., Bonkowski, M. Linking soil microbial nutrient limitation to fertilizer regime and
491 sugar beet yield. *Plant and Soil*, 441, 253–259. doi: 10.1007/s11104-019-04114-w, 2019.
492
493 Li, G., Fan, H. Effect of freeze–thaw on water stability of aggregates in a black soil of Northeast China. *Pedosphere*,
494 24 (2), 285–290. doi:10.1016/S1002-0160(14)60015-1, 2014.
495
496 Li, X., Yang, X., Ma, Y., Hu, G., Hu, X., Wu, X., Wang, P., Huang, Y., Cui, B., Wei, J. Qinghai Lake Basin critical
497 zone observatory on the Qinghai-Tibet Plateau. *Vadose Zone Journal*, 17 (1): 180069. doi:
498 10.2136/vzj2018.04.0069, 2018.
499
500 Liao, J., Yang, X., Dou, Y. Divergent contribution of particulate and mineral-associated organic matter to soil carbon
501 in grassland. *Journal of Environmental Management* 344, 118536. doi:10.1016/j.jenvman.2023.118356, 2023.
502



- 503 Liu, F., Chen, L., Abbott, B.W., Xu, Y., Yang, G., Kou, D., Qin, S., Strauss, J., Wang, Y., Zhang, B., Yang, Y.
504 Reduced quantity and quality of SOM along a thaw sequence on the Tibetan Plateau. *Environmental Research*
505 *Letters* 13, 104017. doi: 10.1088/1748-9326/aae43b, 2018.
- 506
- 507 Liu, F., Kou, D., Chen, Y., Xue, K., Ernakovic, J.G., Chen, L., Yang, G., Yang, Y. Altered microbial structure and
508 function after thermokarst formation. *Global Change Biology*, 27, 4, 823-835. doi:10.1011/gcb.15438, 2021.
- 509
- 510 Liu, F., Qin, S., Fang, K., Chen, L., Peng, Y., Smith, P., Yang, Y. Divergent changes in particulate and mineral-
511 associated organic carbon upon permafrost thaw. *Nature Communications*, 13: 5073. doi:10.1038/s41467-022-
512 32681-7, 2022.
- 513
- 514 Lugato, E., Morari, F., Nardi, S. Relationship between aggregate pore size distribution and organic-humic carbon in
515 contrasting soils. *Soil and Tillage Research*, 103, 153–157. doi: 10.1016/j.still.2008.10.013, 2009.
- 516
- 517 Lugato, E., Simonetti, G., Morari, F., Nardi, S., Berti, A., Giardini, L. Distribution of organic and humic carbon in
518 wet-sieved aggregates of different soils under long-term fertilization experiment. *Geoderma*, 157: 80-85.
519 doi:10.1016/j.geoderma.2010.03.017, 2010.
- 520
- 521 Mako, A., Szabo, B., Rajkai, K., Szabo, J., Bakacsi, Z., Labancz, V., Hernadi, H., Barna, G. Evaluation of soil
522 texture determination using soil fraction data resulting from laser diffraction method. *International*
523 *Agrophysics*, 33, 4, 445-454. doi:10.31545/intagr/113347, 2019.
- 524
- 525 Ma, R., Jiang, Y., Liu, B., Fan, H. Effects of pore structure characterized by synchrotron-based micro-computed
526 tomography on aggregate stability of black soil under freeze–thaw cycles. *Soil and Tillage Research* 207,
527 104855. doi:10.1016/j.still.2020.104855, 2021.
- 528
- 529 Ma, Y., Xie, T., Li, X. Spatial variation of soil organic carbon in the Qinghai Lake watershed, northeast Qinghai-Tibet
530 Plateau. *Catena*, 213, 106187. doi: 10.1016/j.catena.2022.106187, 2022..
- 531
- 532 Mu, C., Abbott, B.W., Norris, A.J., Mu, M., Fan, C., Chen, X., Jia, L., Yang, R., Zhang, T., Wang, K., Peng, X., Wu,



- 533 Q., Guggenberger, G., Wu, X. The status and stability of permafrost carbon on the Tibetan Plateau. *Earth-Science*
534 *Reviews*, 211, 103433. doi:10.1016/j.earthscirev.2020.103433, 2020.
- 535
- 536 Oztas, T., Fayetorbay, F. Effect of freezing and thawing processes on soil aggregate stability. *Catena* 52 (1), 1–8.
537 doi:10.1016/S0341-8162(02)00177-7, 2003.
- 538
- 539 Patel, K.F., Tatariw, C., Macrae, J.D., Ohno, T., Nelson, S.J., Fernandez, I.J. Repeated freeze–thaw cycles increase
540 extractable, but not total, carbon and nitrogen in a Maine coniferous soil. *Geoderma*, 402, 115353.
541 doi:10.1016/j.geoderma.2021.115353, 2021.
- 542
- 543 Peng, X.Q., Zhang, T.J., Frauenfeld, O.W., Wang, K., Cao, B., Zhong, X., Su, H., Mu, C. Response of seasonal soil
544 freeze depth to climate change across China. *Cryosphere*, 11(3): 1059-1073. doi:10.5194/tc-11-1059-2017, 2017.
- 545
- 546 Ping, C., Jastrow, J.D., Jogerson, M.T., Michaelson, G.J., Shur, Y.L. Permafrost soils and carbon cycling. *Soil* 1, 147-
547 171. doi: 10.5194/soil-1-147-2015, 2015.
- 548
- 549 Quigley, M.Y., Negassa, W.C., Guber, A.K., Rivers, M.L., Kravchenko, A.N. Influence of pore characteristics on the
550 fate and distribution of newly added carbon. *Frontiers in Environmental Science*, 6:51.
551 doi:10.3389/fenvs.2018.00051, 2018.
- 552
- 553 Rabot, E., Wiesmeier, M., Schlute, S., Vogel, H.J. Soil structure as an indicator of soil functions: A review. *Geoderma*
554 314, 122-137. doi: 10.1016/j.geoderma.2017.11.009, 2018.
- 555
- 556 Rempel, A.W., van Alst, L.J. Potential gradients produced by pore-space heterogeneities: Application to isothermal
557 frost damage and submarine hydrate anomalies. *Poromechanics V: Proceedings of the Fifth Biot Conferences on*
558 *Poromechanics*, 813–822. doi: 10.1061/9780784412992.098, 2013.
- 559
- 560 Ruamps, L.S., Nunan, N., Pouteau, V., Leloup, J., Raynaud, X., Roy, V., Chenu, C. Regulation of soil organic C
561 mineralisation at the pore scale. *FEMS Microbiology Ecology*, 86 (1), 26–35. doi: 10.1111/1574-6941.12078,
562 2013.



- 563
- 564 Schutter, M.E., Dick, R.P. Microbial community profiles and activities among aggregates of winter fallow and cover-
- 565 cropped soil. *Soil Science Society of America Journal*, 66 (1), 142-153. doi:10.2136/sssaj2002.1420, 2002.
- 566
- 567 Six, J., Bossuyt, H., Degryze, S., Deneff, K. A history of research on the link between (micro)aggregates, soil biota,
- 568 and soil organic matter dynamics. *Soil and Tillage Research*, 79(1):7-31. doi:10.1016/j.still.2004.03.008, 2004.
- 569
- 570 Six, E., Elliott, E., Paustian, K. Soil macroaggregate turnover and microaggregate formation: a mechanism for C
- 571 sequestration under no-tillage agriculture. *Soil Biology and Biochemistry*, 32(14):2099-2103. doi:
- 572 10.1016/S0038-0717(00)00179-6, 2000.
- 573
- 574 Skvortsova, E.B., Shen, E.V., Abrosimov, K.N. The impact of multiple freeze–thaw cycles on the microstructure of
- 575 aggregates from a Soddy-Podzolic soil: a microtomographic analysis. *Eurasian Soil Science*, 51 (2), 190-198.
- 576 doi: 10.1134/S106422931802012, 2018.
- 577
- 578 Song, Y., Zou, Y., Wang, G., Yu, X. Altered soil carbon and nitrogen cycles due to the freeze-thaw effect: A meta-
- 579 analysis. *Soil Biology and Biochemistry*, 109: 35-49. doi: 10.1016/j.soilbio.2017.01.020, 2017.
- 580
- 581 Starkloff, T., Larsbo, M., Stolte, J., Hessel, R., Ritsema, C. Quantifying the impact of a succession of freezing-thawing
- 582 cycles on the pore network of a silty clay loam and a loamy sand topsoil using X-ray tomography. *Catena*, 156,
- 583 365–374. doi: 10.1016/j.catena.2017.04.026, 2017.
- 584
- 585 Strong, E.T., Wever, H.D., Merckx, R., Recous, S. Spatial location of carbon decomposition in the soil pore system.
- 586 *European Journal of Soil Science*, 55 (4), 739–750. doi: 10.1111/j.1365-2389.2004.00639.x, 2004.
- 587
- 588 Sun, T., Mao, X., Han, K., Wang, X., Cheng, Q., Liu, X., Zhou, J., Ma, Q., Ni, Z., Wu, L. Nitrogen addition increased
- 589 soil particulate organic carbon via plant carbon input whereas reduced mineral-associated organic carbon through
- 590 attenuating mineral protection in agroecosystem. *Science of the Total Environment*, 165705.
- 591 doi:10.1016/j.scitotenv.2023.165705, 2023.
- 592



- 593 Tan, B., Wu, F., Yang, W., He, X. Snow removal alters soil microbial biomass and enzyme activity in a Tibetan alpine
594 forest. *Applied Soil Ecology*, 76, 34–41. doi: 10.1016/j.apsoil.2013.11.015, 2014.
595
- 596 Todd-Brown, K.E.O., Randerson, J.T., Hopkins, F., Arora, V., Hajima, T., Jones, C., Shevliakova, E., Tjiputra, J.,
597 Volodin, E., Wu, T., Zhang, Q., Allison, S.D. Changes in soil organic carbon storage predicted by Earth System
598 models during the 21st century. *Biogeosciences*, 11 (8): 2341-23356. doi: 10.5194/bg-11-2341-2014, 2014.
599
- 600 Toosi, E.R., Kravchenko, A.N., Guber, A.K., Rivers, M.L. Pore characteristics regulate priming and fate of carbon
601 from plant residue. *Soil Biology and Biochemistry*, 113, 219–230. doi: 10.1016/j.soilbio.2017.06.014, 2017.
602
- 603 Wang, D., Ma, Y., Niu, Y., Chang, X., Wen, Z. Effects of cyclic freezing and thawing on mechanical properties of
604 Qinghai-Tibet clay. *Cold Regions Science and Technology*, 48:34–43. doi: 10.1016/j.coldregions. 2006. 09. 008,
605 2007.
606
- 607 Wang, E., Cruse, R., Chen, X., Daigh, A. Effects of moisture condition and freeze/thaw cycles on surface soil aggregate
608 size distribution and stability. *Canadian Journal of Soil Science*, 92 (3), 529-536. doi: 10.1007/s40333-017-0009-
609 3, 2012.
610
- 611 Wang, F., Zhang, X., Neal, A.L., Crawford, J.W., Monney, S.J., Bacq-Labreuil, A. Evolution of the transport properties
612 of soil aggregates and their relationship with soil organic carbon following land use changes. *Soil and Tillage
613 Research*, 215, 105226. doi: 10.1016/j.still.2021.105226, 2022.
614
- 615 Wang, R., Hu, X. Pore structure characteristics and organic carbon distribution of soil aggregates in alpine ecosystems
616 in the Qinghai Lake basin on the Qinghai-Tibet Plateau. *Catena* 231, 107359.
617 <https://doi.org/10.1016/j.catena.2023.107359>, 2023.
618
- 619 Wang, X., Wang., C., Fan, X. Mineral composition controls the stabilization of microbially derived carbon and
620 nitrogen in soils: Insights from an isotope tracing model. *Global Change Biology* 30 (1): e17156. doi:
621 10.1111/gcb.17156, 2024.
622



- 623 Wang, Y., Li, S., Xu, Y. Incorporated maize residues will induce more accumulation of new POC in HF compared
624 with that in LF soils: a comparison of different residue types. *Journal of Soil and Sediments*, 20, 3941–3950. doi:
625 10.1007/s11368-020-02718-9, 2020.
- 626
- 627 Witzgall, K., Vidal, A., Schubert, D.I., Hoschen, C., Schweizer, S.A., Buegger, F., Pouteau, V., Chenu, C., Mueller,
628 C.W. Particulate organic matter as a functional soil component for persistent soil organic carbon. *Nature*
629 *Communications*, 12 (1), 1–10. doi: 10.1038/s41467-021-24192-8, 2021..
- 630
- 631 Wu, Q., Zhang, T., Liu, Y. Permafrost temperatures and thickness on the Qinghai-Tibet Plateau. *Global and Planetary*
632 *Change*, 72 (1–2), 32–38. doi:10.1016/j.gloplacha.2010.03.001, 2010.
- 633
- 634 Wu, T., Li, X., Zuo, F., Deng, Y., Hu, G. Responses of soil water dynamics to precipitation events in an alpine meadow
635 ecosystem of the Qinghai Lake Basin based on high-precision lysimeter measurements. *Hydrological Processes*,
636 37(4):e14874. doi:10.1002/hyp.14874, 2023.
- 637
- 638 Wu, Y., Hu, X. Soil open pore structure regulates soil organic carbon fractions of soil aggregates under simulated
639 freeze-thaw cycles as determined by X-ray computed tomography. *Journal of Soil Science and plant nutrition*.
640 2024.
- 641
- 642 Xiao, L., Zhang, Y., Li, P., Xu, G., Shi, P., Zhang, Y. Effects of freeze–thaw cycles on aggregate-associated organic
643 carbon and glomalin-related soil protein in natural-succession grassland and Chinese pine forest on the Loess
644 Plateau. *Geoderma*, 334, 1–8. doi: 10.1016/j.geoderma.2018.07.043, 2019.
- 645
- 646 Yang, Z., Hu, X., Gao, Z., Zhao, Y. Soil macropore networks derived from X-ray computed tomography in response
647 to typical thaw slumps in Qinghai-Tibetan Plateau, China. *Journal of Soil and Sediments*, 21, 2845-2854.
648 doi:10.1007/s11368-021-02983-2, 2021.
- 649
- 650 Yi, Y., Kimball, J.S., Rawlins, M.A., Moghaddam, M., Euskirchen, E.S. The role of snow cover affecting boreal-arctic
651 soil freeze–thaw and carbon dynamics. *Biogeosciences*, 12:5811–5829. doi: 10.5194/bg-12-5811-2015, 2015.
- 652



- 653 Zhang, W., Munkholm, L.J., Liu, X., An, T., Xu, Y., Ge, Z., Xie, N., Li, A., Dong, Y., Peng, C., Li, S., Wang, J. Soil
654 aggregate microstructure and microbial community structure mediate soil organic carbon accumulation:
655 Evidence from one-year field experiment. *Geoderma*, 430, 116324. doi: 10.1016/j.geoderma.2023.116324, 2023.
656
- 657 Zhang, X., Xin, X., Zhu, A., Zhang, J., Yang, W. Effects of tillage and residue managements on organic C
658 accumulation and soil aggregation in a sandy loam soil of the North China Plain. *Catena*, 156, 176–183.
659 doi:10.1016/j.catena.2017.04.012, 2017.
660
- 661 Zhang, Z., Wei, M., Feng, W., Xiao, D., Hou, X. Reconstructions of soil particle composition during freeze-thaw
662 cycling: A review. *Pedosphere* 26 (2), 167-179. doi: 10.1016/S1002-0160(15)60033-9. 2016.
663
- 664 Zhao, Y., Hu, X. How do freeze–thaw cycles affect the soil pore structure in alpine meadows considering soil
665 aggregate and soil column scales? *Journal of Soil Science and Plant Nutrition* 22, 4207-4216. doi:
666 10.1007/s42729-022-01019-z, 2022.
667
- 668 Zhao, Y., Hu, X. A pore-scale investigation of soil aggregate structure responding to freeze–thaw cycles using X-ray
669 computed microtomography. *Journal of Soils and Sediments* 23, 3137-3148. doi: 10.1007/s-11368-022-03539-
670 2, 2023a.
671
- 672 Zhao, Y., Hu, X. Seasonal freeze–thaw processes regulate and buffer the distribution of microbial communities in
673 soil horizons. *Catena*, 231, 107348. doi: 10.1016/j.catena.2023.107348, 2023b.
674
- 675 Zhao, Y., Hu, X., Li, X. Analysis of the intra-aggregate pore structures in three soil types using X-ray computed
676 tomography. *Catena*, 193, 104622. doi: 10.1016/j.catena.2020.104622, 2020.
677
- 678 Zhou, H., Peng, X., Peth, S., Xiao, T. Effects of vegetation restoration on soil aggregate microstructure quantified
679 with synchrotron-based micro-computed tomography. *Soil and Tillage Research* 124: 17-23. doi:
680 10.1016/j.still.2012.04.006, 2012.
681



682 Zhu, E., Li, Z., Ma, L. Enhanced mineral preservation rather than microbial residue production dictates the accrual
683 of mineral-associated organic carbon along a weathering gradient. *Geophysical Research Letters* 51(6):
684 e2024GL108466. doi: 10.1029/2024GL108466, 2024.
685